

Original Article

Effect of Plasma and Gas Nitriding Parameters on Microstructure and Mechanical Properties of DIN 1.2367 Hot Work Tool Steel

Ersin Eser Korkmaz¹, Ali Ari², Bülent Başyigit³ and Ali Bayram⁴

¹ErMir Textile and Machinery Ltd., 16140 Bursa, Turkey

²Department of Weapon Industry Technician, Ostim Technical University, Ankara, Turkey

³MSK Steel Forging Ltd., Karacabey-Bursa, Turkey

⁴Department of Mechanical Engineering, Bursa Uludag University, Gorukle-Bursa, Turkey

Received: 01 September 2022

Revised: 02 October 2022

Accepted: 17 October 2022

Published: 31 October 2022

Abstract - This study investigated the hardness and wear on DIN 1.2367 hot work tool steel after applying plasma and gas nitriding processes under different conditions. The effect of the plasma nitriding process temperature and the N₂:H₂ gas mixture ratio was examined in the first group of specimens, whereas the impact of the gas nitriding nitrogen potential and retention time was investigated in the second group of specimens. In the plasma nitriding process applied to the first group, the increase in the N₂ ratio in the gas mixture significantly increased the hardness and wear properties of the material. In addition, the wear resistance of the specimen with the highest hardness value was increased. Although the nitriding time and potential nitrogen values in the second group had changed, the diffusion depth and hardness distribution were found to be close.

Keywords - Plasma nitriding, Gas nitriding, Friction coefficient, DIN 1.2367 tool steel.

1. Introduction

Tool steels are high alloy steels used to shape other materials. Although tool steels have different rates of carbon content, they contain alloying elements such as Cr, Mo, W, Ti, V, Ni, and Co at a higher rate than other steels depending on their intended use. These steels exhibit high strength, toughness, and wear resistance with applied hardening and tempering heat treatments. Because of these properties, tool steels are widely preferred in manufacturing hot and cold-forming die matrices, punches, injection molds, and sheet metal cutting/punching molds.

Applications in which they are used include contact conditions where various wear mechanisms occur, often due to different tribological parameters. Therefore, tool steels must have high hardness, wear resistance, and superior mechanical properties. Steels for hot work applications must also resist softening and exhibit hardness at high temperatures [1]. The microstructure of tool steel is highly dependent on the heat treatment process and is closely related to the material's wear resistance. Wei et al. focused on the friction, wear behavior, and wear mechanisms of heat-treated and tempered hot work tool steel under various sliding conditions and concluded that wear resistance was related to annealing conditions [2].

Leskovsek et al., on the other hand, studied the effect of austenitization and annealing temperatures on the hardness and fracture toughness of H11 hot work tool steel. The austenitization temperatures (1000, 1020, and 1050 °C) were observed when the specimens were tempered above the secondary hardening temperature. In these cases, significantly lower fracture toughness was obtained for specimens austenitized at 1000 °C and 1050 °C [3]. In addition, after increasing the austenitization temperature, hardness was increased by quenching [4,5].

Surface engineering is a common industrial practice used to extend the life of metals and improve material performance. Nitriding is a thermochemical surface treatment that contributes significantly to fatigue strength, tribological properties, and corrosion resistance. The process involves the diffusion of nitrogen species from different media types leading to the formation of nitrogen-rich phases in the near-surface region [6]. The composition and thickness of the nitrided layers are highly dependent on operating parameters such as processing temperature and time, atmospheric conditions, and substrate composition. Several studies have indicated that fatigue performance [7], tribological properties [8], and corrosion resistance [9] are closely related to these parameters.



Fernandes et al. subjected H13 steel to plasma nitriding at temperatures of 450, 550, and 650 °C. A diffusion zone was observed at the nitriding temperature of 450 °C, whereas a composite layer was produced at 550 °C and 650 °C. Both the surface and bulk hardness decreased as the nitriding temperature increased. In terms of wear and corrosion, it was concluded that a nitriding temperature of 450 °C or 550 °C led to better corrosion properties and that better wear performance was achieved at the nitriding temperature of 650 °C [6]. Leite et al. subjected H13 tool steel discs to plasma nitriding at 400 °C in a mixture of 80% H₂-20% N₂ gas for treatment times of 4 - 36 h. Results showed that longer nitriding time reduced wear volume [8]. Soleimani et al. applied the plasma nitriding process to DIN 1.2210 steel under different temperatures and time conditions. It was concluded that plasma nitriding significantly improved the fatigue life of the steel. Fatigue strength increased with increasing plasma nitriding temperature and time [7]. Bhadraiah et al. applied the plasma nitriding process to Cr-MoV steel at 450 °C and 515 °C temperatures. They reported that the maximum surface hardness of about 1200 HV was reached at 515 °C, and the diffusion depth was ~108 µm [10]. Wen et al. applied plasma nitriding to plastic mold steel at 470, 500, and 530 °C for 4, 8, and 12 h under an atmosphere of 25% N₂ + 75% H₂. The amount of ε-nitride and total nitride increased with the increase in nitriding temperature and time. They found that the material's corrosion resistance increased parallel with the nitriding temperature and time [9].

DIN 1.2367 (X38CrMoV5-3) is a commonly used chromium-molybdenum tool steel. The higher molybdenum content of DIN 1.2367 provides better hot hardness and temper resistance than similar tool steels such as AISI H11 and H13. DIN 1.2367 steel has gained importance in various applications such as gears, cutting knives, mandrel punches, and tool dies because of its hardness and toughness at high temperatures and good resistance to wear and thermal fatigue. The mechanical, friction, and wear properties of DIN 1.2367 tool steel have been extensively investigated in terms of the tempering process and the associated microstructure [11]. In some applications, DIN 1.2367 tool steel is subjected to high cyclic plastic deformation, which causes microchipping and fracture, thus making it essential to characterize its fatigue behavior.

Through systematic experiments, Liu et al. macroscopically and microscopically characterized the effects of annealing and plasma nitriding treatments on the low-cycle fatigue behavior of DIN 1.2367 tool steel. Appropriate life estimation approaches were proposed to correlate low-cycle fatigue-life data obtained under various process conditions for this tool steel. As a result, the best fatigue life for the tempered condition was attained at 580 °C, followed by 540 °C, whereas the lowest was found at 620 °C. The fatigue life differences were significantly reduced

for the three-temper conditions with plasma nitriding, and the strain life curves nearly reached convergence. Fractography observations indicated brittle cracking with no obvious cracks on the fatigue-fractured surfaces of the plasma-nitrided specimens [12].

DIN 1.2367 is used extensively in the hot work tool steel metal forging industry. Nitriding processes are applied to increase the surface wear resistance of this steel. Therefore, in this study, plasma and gas nitriding processes were applied to DIN 1.2367 steel under different conditions to examine the wear properties of this steel depending on the nitriding parameters.

2. Material and Methods

The material used in this research was commercially available DIN 1.2367 (X38CrMoV5-3) hot work tool steel with the chemical composition (% by weight) as specified in Table 1. Typical applications of DIN 1.2367 include small and middle-sized die-casting dies for light alloys (aluminum, zamak, brass, and magnesium), dies and molds for thermosets, and thermoplastic injection molding die. Further applications of DIN 1.2367 hot work tool steel include light alloy extrusion tooling (e.g., liners, mandrels, pressure pads, extrusion stems and dies), forging and hot stamping of light and heavy metals, closed dies, punches, stamps, jaws, and hot rolling rolls, as well as hot cutting applications (e.g., circular, straight, and angular cutting blades) [27].

Table 1. Nominal composition of the DIN 1.2367 hot work steel used in this study

C (%)	Si (%)	Mn (%)	P (%)	S (%)	Cr (%)	Mo (%)	V (%)
0.393	0.455	0.380	<0.03	<0.02	4.81	3.2	0.501

Austenitizing temperatures were chosen according to the steel manufacturer's recommendations and the stability of the carbides. The recommended austenitizing temperature for DIN 1.2367 hot work tool steel is 1030 °C. After the final preheating of the test specimens to 850 °C in a horizontal vacuum furnace, they were heated to a final austenitization temperature of 1030 °C at a heating rate of 12 °C/min. They were held at this temperature for 2 h because the specimens had a wall thickness of 30 mm. Quenching was then performed at a rate of 3 °C/s using nitrogen gas at 45 bar pressure. Finally, tempering was applied at 520 °C for 2 h. As a result of these heat treatments, the hardness of the DIN 1.2367 hot work tool steel was 50 HRC.

Five different nitriding processes were applied to the DIN 1.2367 hot work tool steel. Conditions of nitration are shown in Table 2.

The Group-1 specimens were placed on the cathode before the plasma nitriding (PN) process and vacuumed until the process chamber pressure was 2×10^{-2} mbar. Hydrogen

gas was then introduced into the interior until the gas pressure was 2.5 mbar for the "scattering process", which would provide surface cleanliness and roughness suitable for nitriding. Scattering was carried out at 250 °C treatment temperature for 30 min. Following this process, 80% H₂, 20% N₂ for the first specimen, 80% H₂, and 20% N₂ for the second specimen, and a fixed gas mixture of 20% H₂, 80% N₂ for the third specimen were given into the vacuum chamber. Nitriding was carried out at a process pressure of 2.5 mbar. Plasma nitriding processes were applied at two different temperatures for 10 h. The application temperature was 540 °C for the first specimen, 500 °C for the second, and 500 °C for the third. After the nitriding process was completed, nitrogen gas at 3 mbar was injected into the vacuum chamber. The specimens were cooled to room temperature in a vacuum environment.

The gas nitriding (GN) process was applied to the Group-2 specimens in different laboratories. The nitriding temperature for both specimens was determined as 500 °C. The nitrogen potential working parameter of the first specimen was determined as $Kn = 4(\text{atm})^{-1/2}$, and the nitriding time was 12 h, whereas the nitrogen potential of the second specimen was determined as $Kn = 18(\text{atm})^{-1/2}$, and the nitriding time was 20 h (Table 3). The oven was first preheated and equilibrated to a preset temperature (450 °C), which took approximately 3 h and 10 min. The air in the retort was replaced with a mixture of ammonia and nitrogen gas. The control system calculated the filling time (1 h and 40 min) based on the furnace volume and the incoming gas flow. At each process step, temperature and gas flow was controlled to reach the set point Kn values dependent on ammonia.

Table 2. Plasma nitriding test parameters

Test Specimens	Temperature	Time	N ₂ :H ₂	Pressure
PN1	540 °C	10 h	1:4	250 Pa
PN2	500 °C	10 h	1:4	250 Pa
PN3	500 °C	10 h	4:1	250 Pa

Table 3. Gas nitriding test parameters

Test Specimens	Temperature	Time	Kn
GN1	500 °C	12 h	$Kn = 4$
GN2	500 °C	20 h	$Kn = 18$

For microstructure studies and hardness distribution, the starting material and processed and nitrided specimens were sanded with 180, 320, 400, 600, and 1000 grit sandpaper in a polishing device. After this process, they were polished with a broadcloth using 6- μm and 1- μm diamond pastes.

Microstructure studies were carried out under a Nikon LV 150 light microscope. The Metkon MH-3 Vickers hardness-testing machine with a load range of 0.01-1 kg was used for hardness measurements under a 50-g load and test time of 10 s. Hardness measurements were made on the

specimens at 50, 100, 150, 200, 250, and 300 μm . Five measurements were made for each hardness value, and their arithmetic average was taken. In this study, the nitriding depth according to the DIN 50 190/3 standard was accepted as the depth at which the hardness value of 50 HV above the core hardness was reached.

The wear tests were conducted in a dry friction environment without removing the wear product residues. Friction speeds were chosen as 12.4 mm/s and 5 mm/s. The load was selected as 15 N, and the data acquisition time was 4 s. The trace diameter was determined as 18 mm. Before and after each wear test, the specimens were weighed on a precision scale, and the mass loss during the test was recorded. The wearing distance was 45 m.

3. Results and Discussion

3.1. Microstructure and Hardness

Figure 1 shows the microstructure of the DIN 1.2367 tool steel as-received (AR) and after heat treatment (HT). As seen in Figure 1a, AR consists of ferrite and pearlite phases. In Figure 1b, small precipitate particles are observed in the internal structure of the tempered steel with a martensite phase in the internal structure. Despite the improvement of the DIN 1.2367 steel, the martensite phase in the internal structure was related to the short curing time.

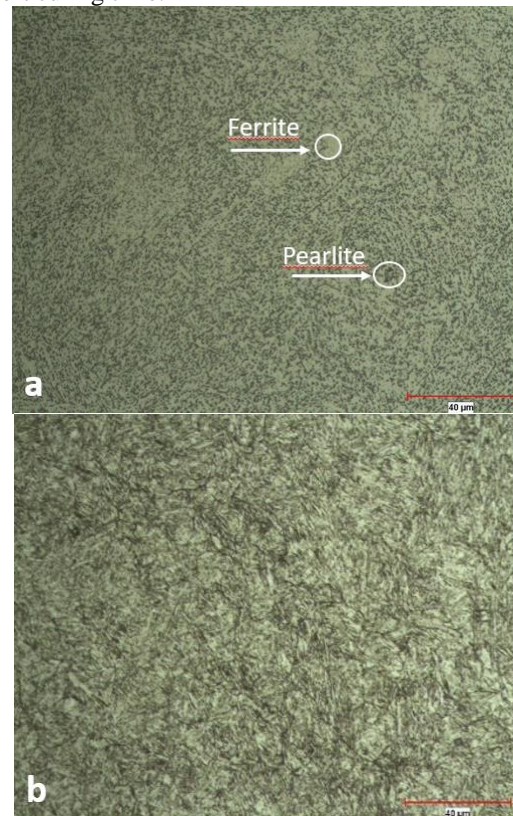


Fig. 1 Microstructure of DIN 1.2367 tool steel under the optical microscope: a) AR, b) HT

The microstructure images in Figures 2-6 show two different regions inwards from the surface. These regions consist of the diffusion layer and the matrix region. The matrix region has a martensitic structure. When the matrix region is carefully examined, precipitate particles are observed in the internal structure. Three points will be considered here: 1) the effect of plasma nitriding temperature on the DIN 1.2367 hot tool steel when gas-mixing ratios are kept constant, 2) the impact of the gas mixture when the plasma nitriding temperature is kept constant, and 3) the effect of changing the nitrogen potential ratio of the material in the gas nitriding process. Figures 2 and 3 show the cross-section of the Group-1 PN1 and PN2 specimens under an optical microscope. The thickness of the diffusion layer of the PN1 specimen subjected to plasma nitriding at 540 °C at a constant N_2/H_2 (1:4) ratio was 215.7 μm (Figure 2a), and the thickness of the diffusion layer of the PN2 specimen subjected to plasma nitriding at 500 °C was 188.8 μm (Figure 3a). As was expected, a deeper diffusion layer was observed at high nitriding temperatures. In the nitriding at 500 °C, there was a weak contrast between the surface region and the core of the specimen. Microhardness measurements were applied to confirm the transition between the diffusion zone and the inner core.

At 550 °C, a more intense contrast can be observed between the surface region and the core of the specimen. The nitrided layer contains fine iron nitrides inside the grains and at the grain boundaries. It is impossible to distinguish the compact composite layer from the main diffusion layer, and needle-like iron nitrides arise in the nitrided layer at both processing temperatures. However, the white layer is slightly more pronounced in the nitrided specimens at 550 °C (Figures 2b and 3b). At a constant temperature of 500 °C, the thickness of the diffusion layer was 188.8 μm with the N_2/H_2 ratio of 1:4 (Figure 3a), whereas the thickness of the diffusion layer was 215.7 μm with the N_2/H_2 ratio of 4:1 (Figure 4a). In the plasma nitriding process performed by Podgornik et al. on an AISI H11 workpiece, it was observed that the thickness of the diffusion layer increased when the N_2 ratios were raised [4], thus supporting the results obtained in our study. Nitriding at 500 °C with the N_2/H_2 ratio of 4:1 (Figure 4b) resulted in a thin white surface layer plus a thick diffusion zone. The distinction between the diffusion zone and the substrate was more apparent in this case.

Additionally, thin elongated precipitates caused by grain boundary precipitation were seen in the diffusion zone. As shown in Figures 3-4, when plasma nitriding occurs at the N_2/H_2 ratio of 1:4 and 500 °C, no white layer is formed, but at the N_2/H_2 ratio of 4:1 and 500 °C, a white layer is formed. This indicates that the thickness of the white layer depends on the nitrogen-hydrogen ratio. The studies of Saulo and Lu support this situation [14,15]. The thickness of the diffusion layer of the Group-2 specimen subjected to $Kn = 4$ and GN treatment for 12 h. at 500 °C was 200 μm (Figure 5a). The

thickness of the layer was 200.7 μm at $Kn = 18$ (Figure 6a). This result shows that the nitriding depth was independent of the nitriding nitrogen potential (Kn). This aligns with the study of Mridha and Khan (2008) [16].

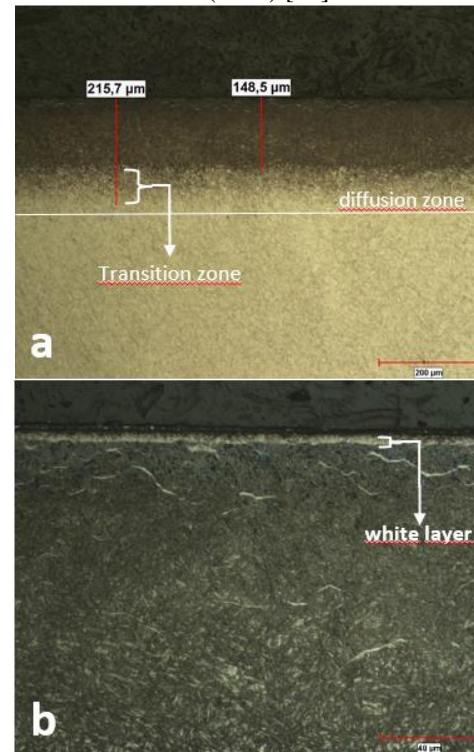


Fig. 2 Optical microscope image of the plasma-nitrided specimen PN1 at 540 oC for 10 h (N_2/H_2 :1/4)

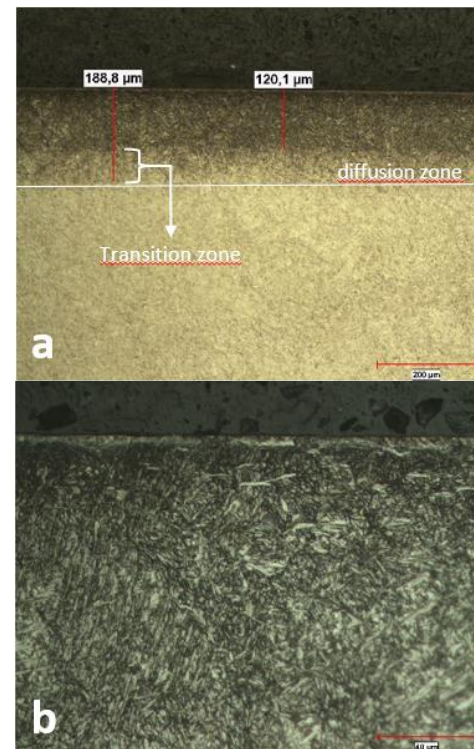


Fig. 3 Optical microscope image of the plasma-nitrided specimen PN2 at 500 oC for 10 h (N_2/H_2 :1/4)

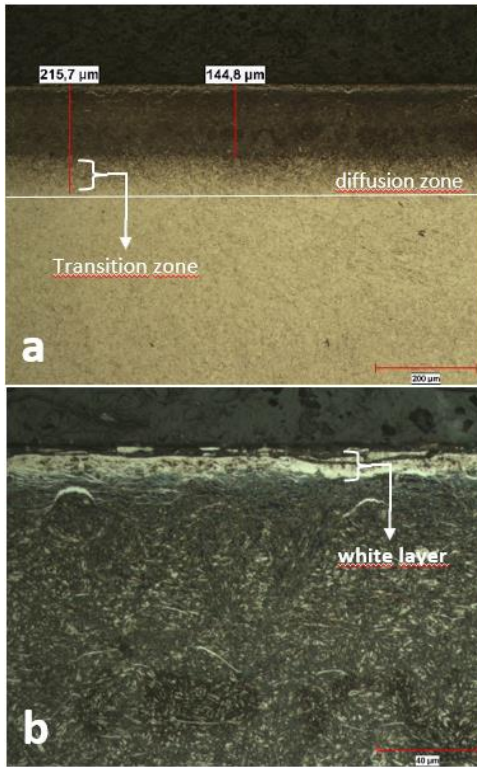


Fig. 4 Optical microscope image of the plasma-nitrided specimen PN3 at 500 oC for 10 h (N₂/H₂:4/1)

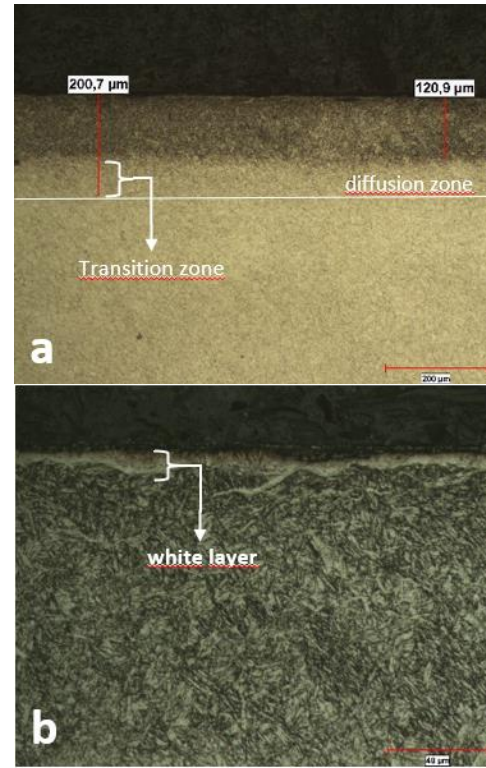


Fig. 6 Optical microscope image of the gas-nitrided specimen GN2 at 500 oC for 12 h (Kn:18)

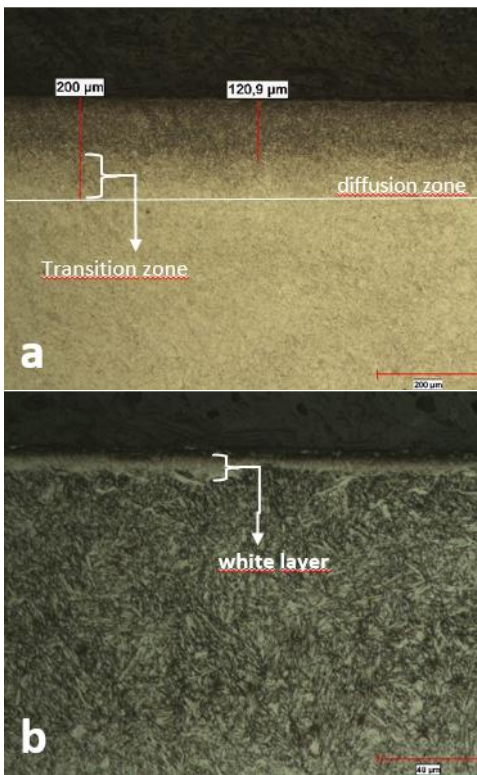


Fig. 5 Optical microscope image of the gas-nitrided specimen GN1 at 500 oC for 12 h (Kn:4)

3.2. Hardness Measurements

The average hardness of the starting material was measured as 196.28 HV and that of the tempered steel as 514.46 HV. Figure 7 shows that the surface hardness of the materials decreased as the nitriding temperature increased. The hardness value of PN2 was 1088.16 HV, and PN1 was 1040.72 HV. Karimzadeh et al. investigated the effect of time and temperature on the plasma nitriding behavior of AISI H13 hot work tool steel. They applied the nitriding process with a 25% N₂-75% H₂ gas mixture and showed that the near-surface hardness decreased with the increase of the treatment temperature [17]. Forati Rad et al. encountered similar results and attributed this to the exposure of the steel substrate to the effect of increased tempering [18]. In the present study, the surface hardness of the PN2 specimen, which was nitrided at 540 °C, was reduced because it was subjected to increased tempering. The surface hardness value of GN1 was 1070.2 HV, and that of GN2 was 1188.6. According to these results, the surface hardness increased in parallel with the nitriding potential. Mridha also reported similar results [16]. The high hardness of this resulting nitrided layer was attributed to the precipitation of the excellent dispersion of CrN and to the maximum surface hardness that increased with the increase in the chromium content, i.e., to the increase in the density of the CrN precipitation at the surface [19].

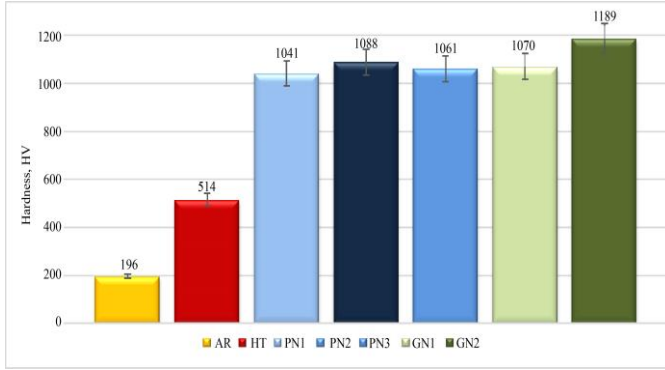


Fig. 7 Hardness results of the test specimens

The hardness distribution and nitriding depth of the plasma nitrided PN1 and PN2 specimens are shown in Figure 8. The hardness distribution of the PN1 and PN2 specimens indicates that the increase in nitriding temperature did not cause a significant change in the hardness distribution. Bhadraiah et al. [10] applied the plasma nitriding process to specimen number one at 515 °C for 10 h. and specimen number two at 450 °C for 10 h and observed the hardness distribution of the specimens was very similar. Podgornik et al. found that altering the plasma activation markedly affected the hardness distribution [4]. Nitrogen ions diffuse inward from the material surface with the plasma nitriding process, forming a nitrided zone. Nitrogen dissolves in steel as interstitial atoms and forms precipitates of alloying elements and nitrides. Nitride precipitates (chrome, molybdenum, vanadium nitride, etc.) disrupt the lattice, create stress fields due to incompatibility with the matrix structure, and compress the dislocations, resulting in a significant increase in hardness. Therefore, when the N_2 ratio is increased in the plasma nitriding process, the thickness and hardness of the diffusion layer of the material also increase [20]. In our study, when the PN2 and PN3 specimens were compared, the N_2/H_2 ratio of the PN2 specimen was 1:4, and that of the PN3 specimen was 4:1. The intense nitriding atmosphere ($N_2 = 80\%$) significantly increased the hardness distribution [21].

The effects of different nitriding nitrogen potentials on the hardness distribution are shown in Figure 8. Here, at 500 °C nitriding temperature, the hardness distribution remained constant for both nitriding nitrogen potentials as the nitriding nitrogen potential increased. Therefore, the hardness distribution was independent of the nitriding potential (Figure 8) but was related to the surface hardness, as mentioned above (Figure 7) [19,26].

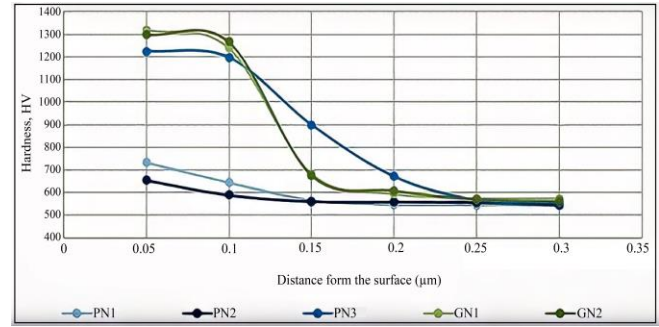


Fig. 8 Hardness distribution of plasma- and gas-nitrided DIN 1.2367 steel specimens

3.3. Wear Resistance

The friction coefficient variation graphs from the wear tests are given in Figures 9 - 18 for a 15-N load. The friction coefficient increased rapidly from the start of the test in both the starting material and nitrided specimens and, after a short time, switched to steady-state conditions (Figures 9 - 18). The plasma nitriding results show that the friction properties were improved, with the lowest friction values found in the PN3 specimen (Figure 13). Hard, abrasive particles are released during friction, disrupting the contact conditions. Thus, the coefficient of friction changes and the abrasive wear character emerges (Figures 19 - 24). This situation was also reported in the study of Karaoğlu [26]. The results of tests performed at a 15-N load and 5-mm/s and 12.4-mm/s sliding speeds show similar characteristics. When the friction coefficients were compared, they were found to be directly related to the surface hardness. The friction coefficients of specimens GN1, GN2, and PN3, which have roughly equal hardness distribution at 0.05 μm , were the lowest. Because the hardness distribution of PN1 and PN2 at 0.05 μm was roughly equal, the friction coefficients were also very similar in these two specimens. These specimens' initial friction coefficient value was high due to surface roughness but was reduced to a steady value after about 10 m sliding distance [23]. Because of the high hardness of the sublayer, the oxide layers were protected and acted as a solid lubricant that effectively reduced the contact area, decreasing the friction coefficient and the wear rate of these specimens [24,25]. The nitriding process temperatures of PN1 and PN2 were 500 °C and 550 °C, respectively, so the 50 °C nitriding process temperature difference had no significant effect on the friction coefficient. However, increasing the N_2 ratio in the gas mixture to 4:1 significantly improved the friction coefficient. With regard to the process parameters of the GN1 and GN2 specimens subjected to the gas nitriding process, changing the K_n ratio did not significantly affect the friction coefficient.

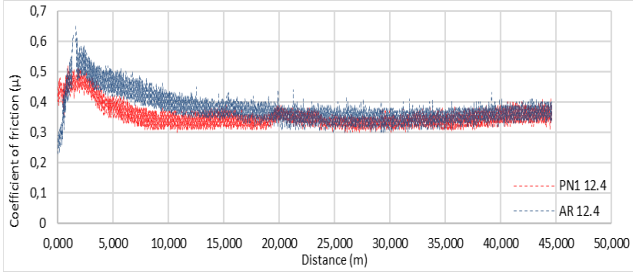


Fig. 9 Friction coefficient changes of AR and PN1 specimens at 12.4 mm/s sliding speed

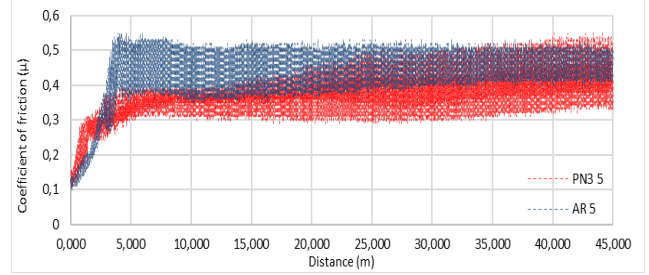


Fig. 14 Friction coefficient changes of AR and PN3 specimens at 5 mm/s sliding speed

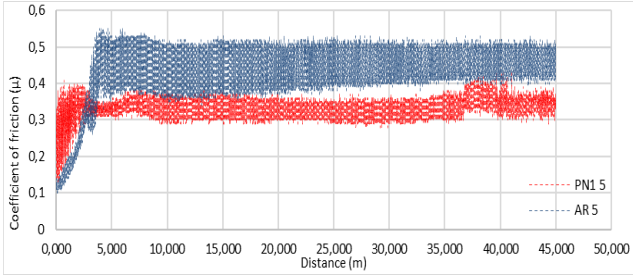


Fig. 10 Friction coefficient changes of AR and PN1 specimens at 5 mm/s sliding speed

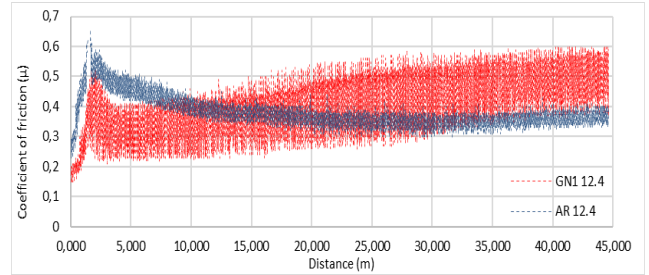


Fig. 15 Friction coefficient changes of AR and GN1 specimens at 12.4 mm/s sliding speed

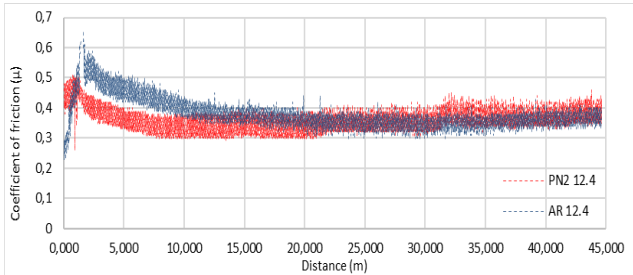


Fig. 11 Friction coefficient changes of AR and PN2 specimens at 12.4 mm/s sliding speed

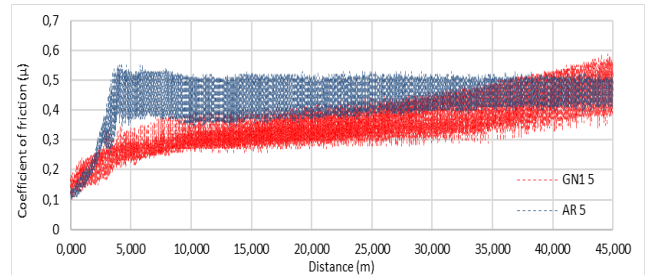


Fig. 16 Friction coefficient changes of AR and GN1 specimens at 5 mm/s sliding speed

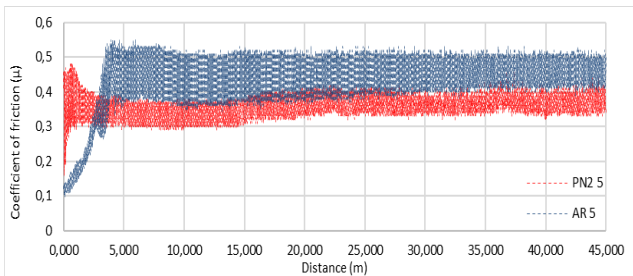


Fig. 12 Friction coefficient changes of AR and PN2 specimens at 5 mm/s sliding speed

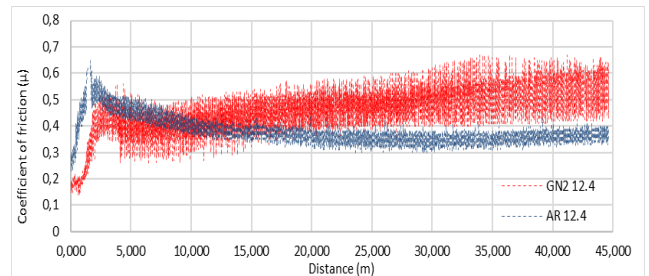


Fig. 17 Friction coefficient changes of AR and GN2 specimens at 12.4 mm/s sliding speed

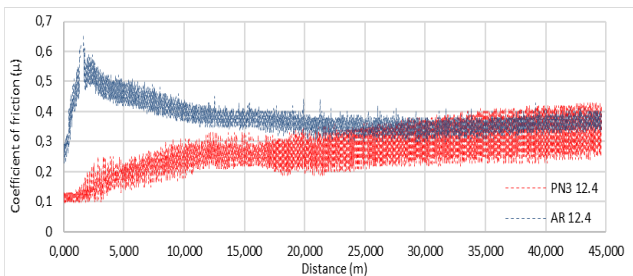


Fig. 13 Friction coefficient changes of AR and PN3 specimens at 12.4 mm/s sliding speed

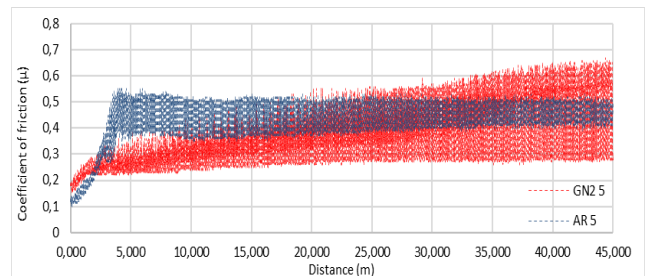


Fig. 18 Friction coefficient changes of AR and GN2 specimens at 5 mm/s sliding speed

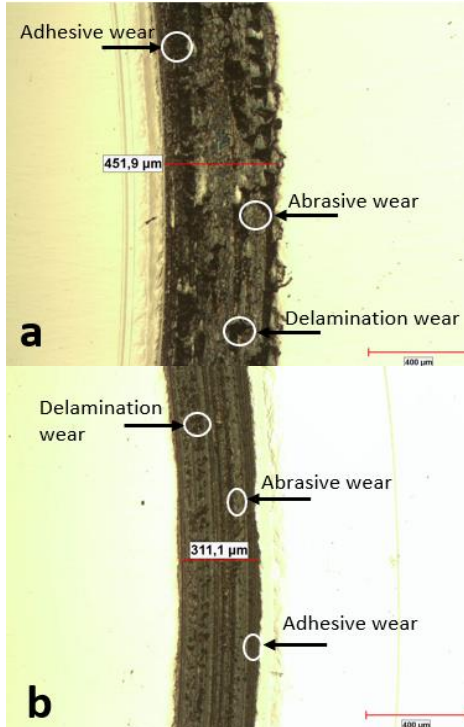


Fig. 19 Optical microscope image of the wear groove and track width for AR specimen: (a) 12.4 mm/s, (b) 5 mm/s

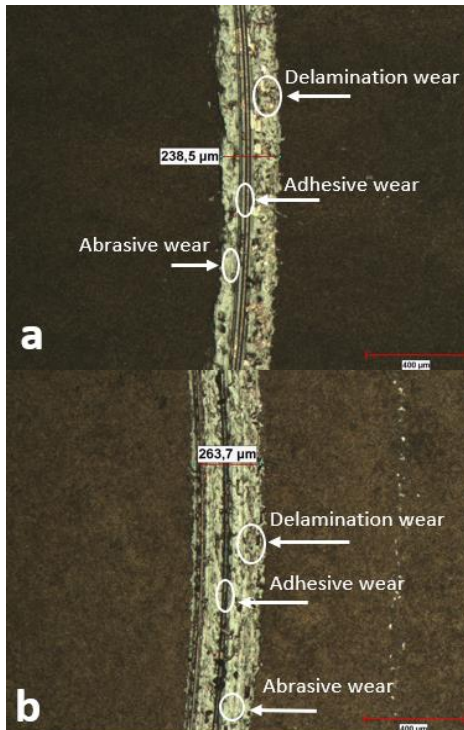


Fig. 20 Optical microscope image of the wear groove and track width for PN1 specimen: (a) 12.4 mm/s, (b) 5 mm/s

Figures 19-24 show that, according to this study's nitriding type and parameters, the DIN 1.2367 nitrided steel exhibited much higher wear resistance than the AR. The 12.4

mm/s PN3 test specimen (Figure 22a) exhibited the lowest extent of wear trace, which was 2.7 fold lower compared to the wear trace of AR (Figure 19).

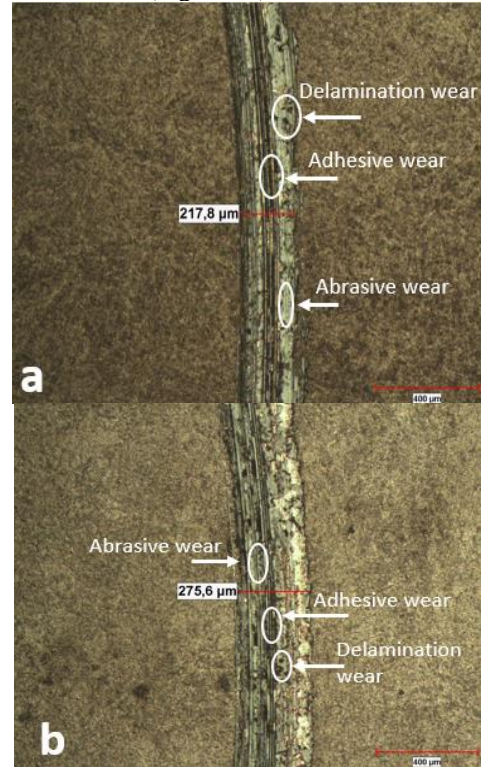


Fig. 21 Optical microscope image of the wear groove and track width for PN2 specimen: (a) 12.4 mm/s, (b) 5 mm/s

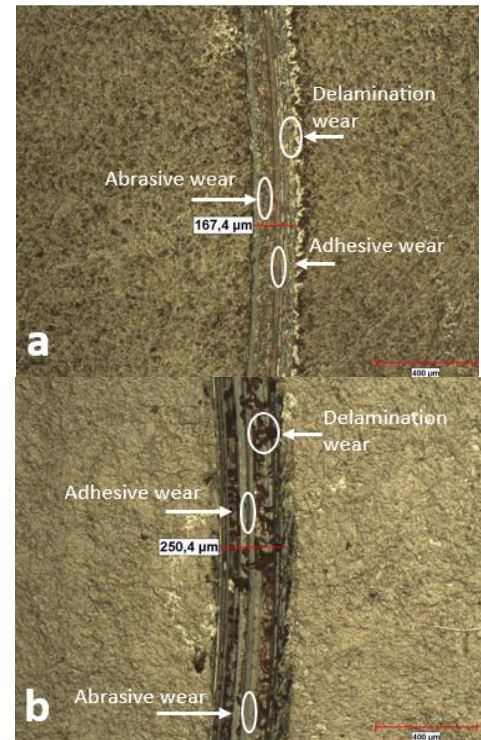


Fig. 22 Optical microscope image of the wear groove and track width for PN3 specimen: (a) 12.4 mm/s, (b) 5 mm/s

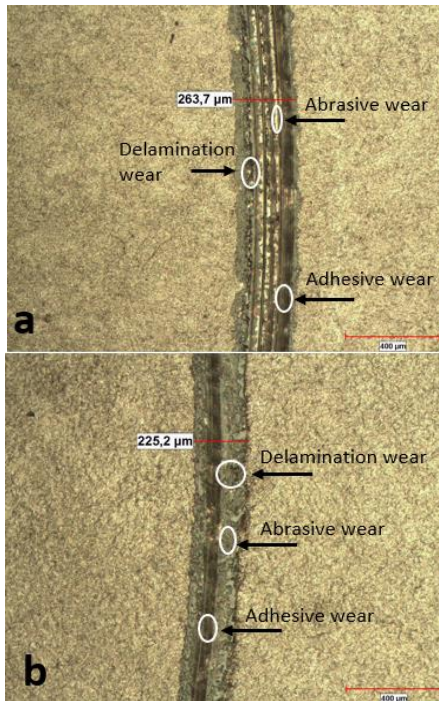


Fig. 23 Optical microscope image of the wear groove and track width for GN1 specimen: (a) 12.4 mm/s, (b) 5 mm/s

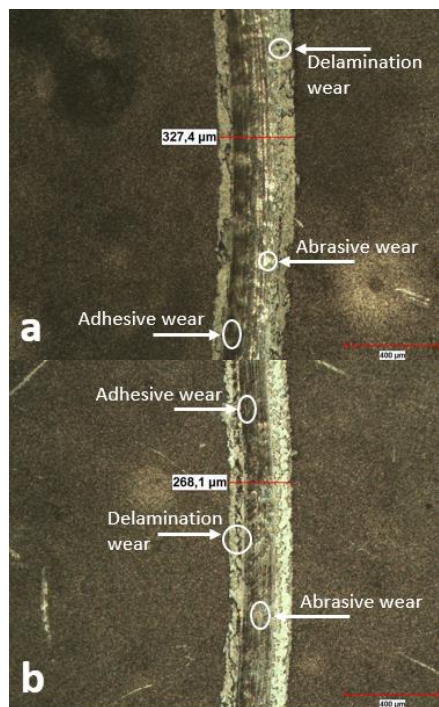


Fig. 24 Optical microscope image of the wear groove and track width for GN2 specimen: (a) 12.4 mm/s, (b) 5 mm/s

When the microscope images of the AR specimen are examined (Figure 19), abrasive wear can be seen in addition to adhesive wear. When the wear areas of the analyzed specimens are compared, the nitration process is shown to contribute to the tribological properties of the specimens. The wear trace of the GN2 specimen (Figure 24), which had

the highest surface hardness, was wider than that of the other nitrated specimens. The hard and brittle structure formed with the applied load caused fractures and abrasive fragments. Intense abrasive and adhesive wear can be seen in the microstructure images. In addition, since the wear products were not removed during the experiment, the particles in question increased the wear in the test system. Figures 19 - 24 show that these particles adhered to the test specimen with abrasive effects causing the formation of cavities. The PN3 specimen exhibited the lowest amount of wear trace, i.e., the best wear resistance was seen in the PN3 specimen. It was because of the intense nitriding atmosphere ($N_2 = 80\%$). The highest hardness was seen in the PN3 specimen at a depth of 0.15 μm, which provided high wear resistance just below the surface. Therefore, it exhibited higher abrasion resistance compared to the other specimens.

4. Conclusion

This study examined the effect of the nitriding conditions on the hardness, diffusion depth, and wear properties of DIN 1.2367 hot work tool steel.

The surface hardness decreased with the increased temperature of the plasma nitriding process. This reduction in hardness was attributed to the high-temperature tempering of the substrate. The hardness distribution in the layers of the PN3 specimen (with plasma nitriding conditions of 500 °C and the $N_2:H_2$ gas mixture ratio of 4:1) was higher than for PN1 and PN2.

Among all the specimens, the highest surface hardness under all nitriding conditions was obtained from the GN2 specimen (gas nitriding at 500 °C for 20 h).

When the N_2 ratio in the N_2/H_2 gas mixture was increased from 1:4 to 4:1 in the plasma nitriding process, the diffusion layer and hardness values increased significantly.

A white layer was formed in the PN3 specimen at 500 °C with the N_2/H_2 gas mixture ratio of 4:1. However, no white layer was formed in the PN2 specimen at 500 °C with the N_2/H_2 gas mixture ratio of 1:4.

The nitriding hardening of the DIN 1.2367 hot work tool steel significantly contributed to the wear resistance property of the material compared to the untreated steel.

The wear properties were very close at the nitriding temperatures of 500 °C and 540 °C. However, as seen in the PN3 specimen, when the N_2 in the N_2/H_2 gas mixture ratio was increased from 1:4 to 4:1, the friction coefficient and wear traces were significantly reduced, with the lowest friction coefficient and wear trace observed in the PN3 specimen.

In the gas nitriding process, the hardness distribution was independent of the nitriding nitrogen potential; however, the surface hardness increased with the increase of the nitriding nitrogen potential.

References

- [1] B. Yalçın, B. Ergene, and S. Nar, “Failure Analysis in Injection Gate Brush Manufactured from 1.2367 Tool Steel and Prevention of Failure with Geometric Design Improvement,” *International Journal of Science & Technoledge*, vol. 11, no. 3, pp. 137–146, 2019. [[Google Scholar](#)]
- [2] M.X. Wei et al., “Effect of Tempering Conditions on Wear Resistance in Various Wear Mechanisms of H13 Steel,” *Tribology Letters*, vol. 44, no. 7-9, pp. 898–905, 2011. [[CrossRef](#)] [[Google Scholar](#)] [[Publisher Link](#)]
- [3] Vojteh Leskovšek, Borivoj Šuštaršič, and Gorazd Jutriša, “The Influence of Austenitizing and Tempering Temperature on the Hardness and Fracture Toughness of Hot-Worked H11 Tool Steel,” *Journal of Materials Processing Technology*, vol. 178, no. 1-3, pp. 328-334, 2006. [[CrossRef](#)] [[Google Scholar](#)] [[Publisher Link](#)]
- [4] B. Podgornik et al., “Vacuum Heat Treatment Optimization for Improved Load Carrying Capacity and Wear Properties of Surface Engineered Hot Work Tool Steel,” *Surface and Coatings Technology*, vol. 261, pp. 253–261, 2015. [[CrossRef](#)] [[Google Scholar](#)] [[Publisher Link](#)]
- [5] Božo Skela et al., “Wear Behaviour and Correlations to the Microstructural Characteristics of Heat Treated Hot Work Tool Steel,” *Wear*, vol. 426-427, pp. 1118-1128, 2019. [[CrossRef](#)] [[Google Scholar](#)] [[Publisher Link](#)]
- [6] F.A.P. Fernandes et al., “On the Wear and Corrosion of Plasma Nitrided AISI H13,” *Surface and Coatings Technology*, vol. 381, pp. 125216, 2020. [[CrossRef](#)] [[Google Scholar](#)] [[Publisher Link](#)]
- [7] S.M.Y. Soleimani et al., “The Effect of Plasma Nitriding on the Fatigue Behavior of DIN 1.2210 Cold Work Tool Steel,” *Materials & Design*, vol. 35, pp. 87-92, 2012. [[CrossRef](#)] [[Google Scholar](#)] [[Publisher Link](#)]
- [8] M. V. Leite et al., “Wear Mechanisms and Microstructure of Pulsed Plasma Nitrided AISI H13 Tool Steel,” *Wear*, vol. 269, no. 5-6, pp. 466–472, 2010. [[CrossRef](#)] [[Google Scholar](#)] [[Publisher Link](#)]
- [9] Dong Cherng Wen, “Microstructure and Corrosion Resistance of the Layers Formed on the Surface of Precipitation Hardenable Plastic Mold Steel by Plasma-Nitriding,” *Applied Surface Science*, vol. 256, no. 3, pp. 797–804, 2009. [[CrossRef](#)] [[Google Scholar](#)] [[Publisher Link](#)]
- [10] D. Bhadraiah et al., “Plasma-Based Nitriding of Tool Steel for the Enhancement of Hardness,” *Materials Today: Proceedings*, no. 46, pp. 940–943, 2021. [[CrossRef](#)] [[Google Scholar](#)] [[Publisher Link](#)]
- [11] I. Y. Malik et al, “Microstructure and Wear Behaviour of High Alloyed Hot-Work Tool Steels 1.2343 and 1.2367 Under Thermo-Mechanical Loading,” *IOP Conference Series: Materials Science and Engineering*, vol. 629, no. 1, 2019. [[CrossRef](#)] [[Google Scholar](#)] [[Publisher Link](#)]
- [12] C. C. Liu, J. H. Wu, and C. C. Kuo, “Low-Cycle Fatigue of DIN 1.2367 Steels in Various Treatments,” *Fracture of Nano and Engineering Materials and Structures*, vol. 387, pp. 217–218, 2006. [[CrossRef](#)] [[Google Scholar](#)] [[Publisher Link](#)]
- [13] Raju Kamminana, and Venkatasubbaiah Kambagowni, "Modeling and Optimization of Process Parameters of Friction Stir Welding of Al-Li Alloy AA2050 by Response Surface Methodology," *International Journal of Engineering Trends and Technology*, vol. 69, no. 5, pp. 208-227, 2021. [[CrossRef](#)] [[Google Scholar](#)] [[Publisher Link](#)]
- [14] Saulo Cordeiro Lima, Ruth Hinrichs, and Marcos Antonio Zen Vasconcellos, “The Influence of Nitrogen to Hydrogen Ratio and Temperature on the Thickness and Phase Composition in Plasma Nitrided Ti-6AL-4V,” *Matter Magazine*, vol. 24, 2019. [[CrossRef](#)] [[Google Scholar](#)] [[Publisher Link](#)]
- [15] Lu Song et al., “Effect of Nitrogen Hydrogen Ratio on Plasma Nitriding for 38crmoal,” *Acta Metallurgica Slovaca*, vol. 24, no. 3, pp. 229–233, 2018. [[CrossRef](#)] [[Google Scholar](#)] [[Publisher Link](#)]
- [16] Shahjahan Mridha, “Gas Nitriding of EN40B Steel with Highest Growth Rate of the Case and Reduced White Layer Formation,” *International Journal of Microstructure and Materials Properties*, vol. 2, no. 1, pp. 54–63, 2007. [[CrossRef](#)] [[Google Scholar](#)] [[Publisher Link](#)]
- [17] S. Karimzadeh, F. Mahboubi, and G. Daviran, “Plasma Nitriding Behavior of Din 1.2344 Hot Work Tool Steel,” *Iranian Journal of Materials Science and Engineering*, vol. 17, no. 4, pp. 1-9, 2020. [[Google Scholar](#)] [[Publisher Link](#)]
- [18] H. Forati Rad, A. Amadeh, and H. Moradi, “Wear Assessment of Plasma Nitrided AISI H11 Steel,” *Materials & Design*, vol. 32, no. 5, pp. 2635–2643, 2011. [[CrossRef](#)] [[Google Scholar](#)] [[Publisher Link](#)]
- [19] S. Mridha, and A. A. Khan, “The Effects of Process Variables on the Hardness of Nitrided 3% Chromium Steel,” *Journal of Materials Processing Technology*, vol. 201, no. 1–3, pp. 325–330, 2008. [[CrossRef](#)] [[Google Scholar](#)] [[Publisher Link](#)]
- [20] M. Berg et al., “On Plasma Nitriding of Steels,” *Surface and Coatings Technology*, vol. 124, no. 1, pp. 25–31, 2000. [[CrossRef](#)] [[Google Scholar](#)] [[Publisher Link](#)]
- [21] M.C. İğdil, and M. Tosun L, “Micro and Nano Effects of Plasma Nitridation on Material Properties of 316L Austenitic Stainless Steel,” *Journal of Machine Engineering*, vol. 53, no. 630, pp. 54-68, 2012.
- [22] Haider Sh. Wahad, Qasim K. Salman, and Noor Emad Kareem, "Free Rolling Friction Model of the Femoral Component on the Tibial Plateau in Knee Prosthesis," *International Journal of Engineering Trends and Technology*, vol. 70, no. 5, pp. 201-208, 2022. [[CrossRef](#)] [[Google Scholar](#)] [[Publisher Link](#)]

- [23] Mehmet Karakan, Akgün Alsaran, and Ayhan Çelik, “Effects of Various Gas Mixtures on Plasma Nitriding Behavior of AISI 5140 Steel,” *Materials Characterization*, vol. 49, no. 3, pp. 241–246, 2002. [[CrossRef](#)] [[Google Scholar](#)] [[Publisher Link](#)]
- [24] Jianqun Yang et al., “Microstructural and Tribological Characterization of Plasma- and Gas-Nitrided 2Cr13 Steel in Vacuum,” *Materials & Design*, vol. 32, no. 2, pp. 808–814, 2011. [[CrossRef](#)] [[Google Scholar](#)] [[Publisher Link](#)]
- [25] R. L. Liu, and M. F. Yan, “Improvement of Wear and Corrosion Resistances of 17-4PH Stainless Steel by Plasma Nitrocarburizing,” *Materials & Design*, vol. 31, no. 5, pp. 2355–2359, 2010. [[CrossRef](#)] [[Google Scholar](#)] [[Publisher Link](#)]
- [26] Serdar Karaoğlu, “Structural Characterization and Wear Behavior of Plasma-Nitrided AISI 5140 Low-Alloy Steel,” *Materials Characterization*, vol. 49, no. 4, pp. 349–357, 2003. [[CrossRef](#)] [[Google Scholar](#)] [[Publisher Link](#)]
- [27] Michael Bischof et al., “On the Overaging Behaviour of Tool Steel X38 CrMoV 5-3,” *Materials Science and Engineering: A*, vol. 472, no. 1-2, pp. 148-156, 2008. [[CrossRef](#)] [[Google Scholar](#)] [[Publisher Link](#)]